JAERI-Research
2001-009

HIGH TEMPERATURE INTERACTION BETWEEN ZIRCALOY-4 AND STAINLESS STEEL TYPE 304

March 2001

Fumihisa NAGASE, Takashi OTOMO and Hiroshi UETSUKA

日本原子力研究所
Japan Atomic Energy Research Institute

本レポートは、日本原子力研究所が不定期に公刊している研究報告書です。
入手の問合わせは、日本原子力研究所研究情報部研究情報課（〒319-1195　茨城県那珂郡東海村）あて、お申し越し下さい。なお、このほかに財団法人原子力弘済会資料センター（〒319-1195　茨城県那珂郡東海村日本原子力研究所内）で複写による実費頒布を行っております。

This report is issued irregularly.
Inquiries about availability of the reports should be addressed to Research Information Division, Department of Intellectual Resources, Japan Atomic Energy Research Institute, Tokai-mura, Naka-gun, Ibaraki-ken 〒319-1195, Japan.

編集兼発行　日本原子力研究所

JAERI－Research 2001－009

High Temperature Interaction between Zircaloy-4 and Stainless Steel Type 304

Fumihisa NAGASE, Takashi OTOMO and Hiroshi UETSUKA

Department of Reactor Safety Research
Nuclear Safety Research Center
Tokai Research Establishment
Japan Atomic Energy Research Institute
Tokai-mura, Naka-gun, Ibaraki-ken

(Received January 30, 2001)

The chemical interactions between Zircaloy-4 and stainless steel type 304 were investigated in the temperature range from 1273 to 1573 K to obtain the basic information on the melt progress in the fuel bundle during an LWR severe accident. Reaction layers were formed at the contact interface and grew as the temperature and the time increase. The Zircaloy was preferentially dissolved by the reaction. The SEM/EDX analyses showed that the main process of the reaction was diffusion of Fe, Cr, and Ni into the Zircaloy which resulted in the formation of a Zr-rich eutectic through the tested temperature range. Reaction rates for decrease in the materials thickness were evaluated and the reaction generally obeyed a parabolic rate law. The reaction rate constant was determined at every examined temperature and Arrhenius type rate equations were estimated for the temperature range.

Keywords: LWR, Severe Accident, Core Materials, Zircaloy, Stainless Steel, High Temperature, Chemical Interaction, Eutectic Formation, Elemental Analysis, Reaction Kinetics

ジルカロイ－４とステンレス３０４鋼間の高温反応

日本原子力研究所東海研究所安全性試験研究センター原子炉安全工学部
永瀬　文久・大友　隆・上塚　寛

(2001年1月30日受理)

軽水炉におけるシビアアクシデント時の燃料集合体溶融進展過程に関する基礎的な知見を取得するために、1273～1573K の温度範囲でジルカロイ－４とステンレス 304 鋼間の化学的な相互作用を調べた。接触界面に反応層が形成され、温度上昇及び時間の経過とともに成長した。SEM/EDX 分析により、反応の主過程は Zr リッチの共晶の生成であることが示された。材料の肉厚減少に関する反応速度を評価し、反応が一般に２乗則に従うことを明らかにした。各試験温度について反応速度定数を決定し、アレニウスタイプの反応速度式を求めた。

東海研究所：〒319-1195　茨城県那珂郡東海村白方白根 2-4

Content

目　　次

This is a blank page.

1. Introduction

Since the TMI-2 accident in 1979, degradation and melt progression in the LWR fuel bundle during a severe accident has been investigated in the research reactors [1-5]. Those experiments showed that core component materials melt and chemically interact with each other to form low-melting-temperature liquid phases in the early stage of the bundle degradation. Such liquid phases can dissolve the fuel rods far below the melting temperatures of UO_2 and Zircaloy. This might enhance dissolution of the UO_2 fuel, resulting in the release of a large amount of fission products (FPs). Therefore, the basic information on the core materials interaction as a function of temperature and time has been needed for the severe accident analysis, and separate effect tests in the laboratories have been performed mainly in Forschunszentrum Karlsruhe and Japan Atomic Energy Research Institute [6,7].

Zircaloy and stainless steel are the major metallic components in an LWR core and they keep compatibility during a normal operation. However, they thermodynamically became unstable with each other as the temperature increases. Previous studies reported that the two materials are diffusion-bonded above 1000 K [8,9], and they form a Zr-rich eutectic above 1273 K [10]. The experiments on the bundle degradation [1,2] showed the early failure of the control rod in the PWR type bundle under a severe accident condition. The stainless steel is used as the cladding of a Ag-In-Cd control rod in a PWR, and the Zircaloy is used as the guide tube for the control rod. The failure was probably caused by the liquid phase formation between the stainless steel cladding and the Zircaloy guide tube, since the Ag-In-Cd alloy does not react with the stainless steel cladding [11].

The reaction layer growths in the Zircaloy and the stainless steel were measured, and Arrhenius type rate equations were determined for the temperature range from 1273 to 1473 K in the study by Hofmann et al. [10]. Only this study have provided the reaction kinetics which was essential to the severe accident analysis on the bundle degradation among the previous investigations, because they examined the reaction in a relatively higher temperature range. However, complete liquefaction of the specimen occurred within a very short time above 1473 K due to the very high reaction rate.

It is very important to obtain the reaction kinetics at higher temperatures, where the reaction rate becomes high, for the bundle degradation analysis. Then, the reaction between the Zircaloy and the stainless steel was examined and the reaction kinetics were evaluated in a wider temperature range from 1273 to 1573 K in the present study. The test results are described comparing with those obtained by

Hofmann et al.

2. Material and experimental procedure

A reaction couple consisted of Zircaloy-4 (Zry) crucible and stainless steel type 304 (ss) pellet were used for the isothermal annealing tests. The chemical compositions of Zry and ss are shown in Table 1, and the geometry of the reaction couple is schematically shown in Fig.1. The ss pellet having the same diameter as the inner diameter of the Zry crucible was pressed into the crucible to obtain a good contact condition at the interface. The reaction couple was isothermally heated in an infrared furnace under flowing argon. The annealing temperature ranged from 1273 to 1573 K, and the annealing time ranged from 30 to 2.88×10^4 s (8 h). A rapid heat-up of 10 K/s and short-time holding at a high target temperature were programmed and successfully achieved. A Pt-Pt/13%Rh thermocouple was spot-welded on the bottom surface of the specimen for both the control and the measurement of the temperature. Annealing test with a dummy specimen showed that the temperature difference throughout the reaction couple was less than 10 K. After the isothermal annealing, the reaction couple was rapidly cooled in flowing argon, where the cooling rate in the concerned temperature range was almost equivalent to the heating rate. The reaction couple was vertically cut at its center line, then the cross section was mechanically polished and chemically etched in a solution (55vol% $CH_3CH(OH)COOH$, 19% HNO_3, 19% H_2O, and 7% HF) for metallurgical examination. In addition, elemental analyses were performed with a SEM/EDX (scanning electron microscope/energy dispersive X-ray spectroscopy).

3. Results and discussion

3.1. Macroscopic observation

Figure 2 shows cross sections of reaction couples annealed at 1323 K for 7200 s, 1473 K for 600 s, and at 1573 K for 30 s. Reaction layers were formed between the ss pellets and the Zry crucibles in these reaction couples. The ss pellet kept its original position at 1323 or 1473 K, while it sank in the reaction layer at 1573 K. The densities of the Zry and the ss are estimated to be about 6.4 and 7.5 g/m^3 at the tested

temperatures, and the reaction layer possibly has a medium density between the Zry and the ss. Therefore, the observed position of the ss pellet in the reaction layer suggests that viscosity of the reaction layer was high at 1323 or 1473 K, whereas it was low at 1573 K. The figure also shows that the thickness of the reaction layer at 1323 K is nearly uniform, while that at 1473 and 1573 K changes at positions. Convection occurs in the liquid and it enhances dissolution of materials [12]. Therefore, it can be considered that convection occurred in the liquefied reaction layers at 1473 and 1573 K and locally enhanced dissolution of the Zry and the ss to form the non-uniform reaction layers.

Decrease in the Zry crucible thickness at the bottom side was 785, 1,030, and 1,183 μm respectively in the reaction couples annealed at 1273 K (7200 s), 1473 K (600 s), and 1573 K (30 s). Namely, a larger amount of the Zry was dissolved within a much shorter reaction time at higher temperatures, and this indicates apparent increase of the reaction rate with the temperature increase. Comparison of decrease in thickness of the Zry and the ss shows that Zry was preferentially dissolved. For example, average decrease in the ss thickness was only 180 μm in the reaction couple annealed at 1473 K for 600 s, while that in the Zry thickness was 1,030 μm. This observation agrees with the result reported by Hofmann et al. [10].

3.2 Microscopic observation

3.2.1 Reaction at 1473 K

Figure 3 shows a microstructure of the reaction layer formed by the reaction at 1473 K for 600 s. In the optical microphotograph (Fig.3(a)), only one reaction layer (Layer I) is seen between the Zry and the ss. However, the SEM photograph (Fig.3(b)) shows that a very thin layer (Layers II) of 5 to 10 μ m thick were formed at the ss side. Such a double layer structure was formed commonly in the reaction couples annealed below 1473 K. The measurement of decrease in the materials thickness on the macrophotograph (Fig.2) shows that the initial Zry/ss boundary was located close to the LayerI/II layer boundary in Layer I. Accordingly, most of layer I was formed in the Zry, and Layer II and a part of Layer I was formed in the ss.

Results of the elemental analyses are shown in **Table 2**. The average composition of each layer was determined by the 'integral' analysis for the whole layer thickness, and the elemental concentration near the layer boundary was determined by the analysis for the narrow area of approximately 10 μm×50 μm. The average composition of

Layer I was $Zr_{0.75}Fe_{0.18}Cr_{0.01}Ni_{0.04}Sn_{0.01}Mn_{0.01}$. The analysis data indicates that the main components of the layer were Zr and Fe, and their ratio (Zr:Fe=81.5:18.5) was close to a eutectic composition in the Zr-Fe system (Fig.4)[13]. The formation of the Zr-rich eutectic formation explains the preferential dissolution of the Zry. Hofmann et al.[10] explained that the main process of the of the reaction is diffusion of Fe, Cr, and Ni into the Zry which resulted in the formation of a Zr-rich eutectic. As shown in Table 2, the identical composition was found in the most part of Layer I except for the region adjacent to the Layer I/II boundary. The uniform elemental distribution suggestes that the layer was a liquid phase and mixing occurred by convection. In the narrow region adjacent to Layer II which is shown as Region 'C' in Fig.3(b), the concentrations of Zr and Ni decreased and those of Fe and Cr increased (Table 2). The composition of this region was estimated to be $Zr_{0.35}Fe_{0.30}Cr_{0.32}$ $Mn_{0.02}Ni_{0.01}$. The phase diagram of the Zr-Fe-Cr system [14] shows that the phase with the estimated composition is $Zr(Cr,Fe)_2$ at 1273 K. However, it is unknown whether $Zr(Cr,Fe)_2$ is stable at 1473 K, since the ternary phase diagram is not available for that temperature. The binary phase diagrams of the Zr-Cr and Zr-Fe systems[13] show that solid $ZrCr_2$ and $ZrFe_2$ phases are stable up to about 1900 K. Therefore, it is likely that Region 'C' was solid $Zr(Cr,Fe)_2$ at 1473 K. Various shapes of precipitates are seen in Layer I as shown in Fig.3(a) and 3(b). It was shown in the previous study[10] that they are $Zr_2(Fe,Cr)$, Zr(Fe,Cr), and $Zr_2(Fe,Ni)$ which were formed when the liquid Zr-Fe-Cr-Ni alloy resolidified.

Layer II consisted mainly of Fe and Cr, and it contained a small amount of Zr, Ni, and Mn. This layer was possibly formed in the ss region by interdiffusion of elements. The lowest liquidus temperature of the Fe-Cr binary system is higher than 1770 K[15]. Thus, this layer II is considered to have been solid at the tested temperature.

3.2.2 Reaction at 1523 K

Figure 5(a) shows a microstructure of reaction layers formed by the reaction at 1523 K for 60 s. Two layers, thicker Layer I and thinner layer II, were formed at the interface. The thickness of Layer II relative to Layer I increased at this temperature. Figure 5(b) shows a SEM image of the reaction layers adjacent to the ss. The dendritic structure is seen in Layer I and this clearly indicates that the layer was liquefied at 1523 K. The elemental analysis (Table 3) showed that the average composition of Layer I was nearly equal to the eutectic composition of the Zr-Fe system. Therefore, it can be considered that the main process of the reaction was the formation of the Zr-rich liquid phase at this temperature. Although the elemental analysis (Table 3)

showed that Layer I was homogeneous in most of the thickness, the narrow region consisted of $Zr(Cr,Fe)_2$ was found adjacent to Layer II (shown as Region 'D' in the figure) also at this temperature.

The microstructure of Layer II differed from that below 1473 K (Fig.3(b)). The layer had grain boundaries which were preferentially dissolved by the chemical etching and seemed as stringers. The results of elemental analysis of Layer II are shown in Table 3. The average concentration of the layer was nearly equal to that of the ss. In contrast, the grain boundary in Layer II had a high Zr concentration. Zr might diffuse mainly through the grain boundary, or diffused Zr might be concentrated in the grain boundary during the cooling process.

3.2.3 Reaction at 1573 K

Figure 6 shows a microstructure of the reaction layers formed by the reaction at 1573 K for 30 s. Layer I exhibited quite a different microstructure from that formed below 1523 K, and the microstructure it changed in the thickness. Then, the elemental analyses were performed for seven small regions as shown with numbers in the figure, and the results are shown in Table 4. Region 1 through 3 had the composition seen in Layer I formed below 1523 K. This shows that the Zr-rich eutectic formation occurred at every examined temperature up to 1573 K, though the relative area in the total reaction layer thickness became smaller at 1573 K. Comparison of the elemental compositions at different positions shows that the concentrations of Zr and Sn decreased and those of Fe, Ni, Cr, and Mn increased as the location of the analyzed region was closer to the Layer II. A liquid alloy having concentration gradients of elements could be solidified into those regions during the cooling process. Region 6 and 7 close to Layer II showed apparently the microstructure of the resolidified melt and the layer consisted of Fe and Cr with a certain amount of Zr, Ni, and Mn. This indicates that an (Fe,Cr)-rich eutectic was partly formed between the Zry and the ss at 1573 K.

Layer II at the ss side had the relatively round grains. However, the elemental analysis showed that this layer was the same as that formed at 1523 K, and it contained Zr-rich stringers.

3.3. Evaluation of reaction rate

To evaluate the reaction rate, the decrease in the Zry crucible thickness at the bottom side and the decrease in the ss pellet thickness were measured on the macro

photographs of vertically cut cross sections of reaction couples. As seen in Fig.2, thickness of the reaction layer on the observed specific surface was not uniform, especially in the reaction couples annealed at higher temperatures. Then, the residual cross sectional area of the Zry and the ss was measured with an image analyzer to obtain the average value of decrease in their thickness. Decreases in the Zry and the ss thickness are plotted as a function of square root of isothermal annealing time in Fig.7. The tendency lines were determined by the least squares method. Since a linear relationship was generally seen at every test temperature for the tested time range, a parabolic rate law was used to describe the progression of the reaction. The obtained rate constant in the present study is not 'the parabolic rate law constant' in a strict sense, since very complicated reaction process including the formation of the liquid phases are involved in the reaction. However, it is very useful and necessary to evaluate reaction kinetics for predicting the possible reaction between core materials in a severe accident. Therefore, the reaction rate constant, which corresponded to the slope of the line in the figure, was calculated at every tested temperature.

The calculated reaction rate constants for decreases in the Zry and the ss thickness are summarized in Table 5, and plotted as a function of the reciprocal temperature in Fig.8. The results of the present study are shown with closed and open circles. Although some deviations are seen, the temperature dependence of the reaction rate constants could be represented by a single line for decreases in the Zry and the ss thickness, respectively. Although the (Fe, Cr)-rich eutectic was partly formed in the reaction layer at 1573 K in addition to the Zr-rich eutectic formation, it had no influence on the reaction kinetics for the examined temperature range. Consequently, Arrhenius type rate equations for decrease in the Zry and the ss thickness are as follows:

for decrease in the Zry thickness;

$$x^2/t\ [m^2/s]=3.11\times10^9 \exp(-496000/RT),\ 1273 \text{ to } 1573 \text{ K}$$

for decrease in the ss thickness;

$$x^2/t\ [m^2/s]=1.79\times10^8 \exp(-445000/RT),\ 1273 \text{ to } 1473 \text{ K}$$

where x is decrease in the Zircaloy and the ss thickness, t is time, R=8.314 J/mol K, T is given in K, and the activation energies in J/mol.

The ss pellet often sank in the reaction layer and was dissolved from both the top and the bottom sides at 1523 and 1573 K as seen in Fig.2. Since the beginning of the dissolution at the top cannot be specified, the reaction rate evaluation was not done

for decrease in the ss thickness at those two temperatures.

The data obtained by Hofmann et al.[10] is also plotted as a dotted line in the figure for comparison. They showed higher reaction rate constants above 1373 K for the Zry dissolution and lower rate constants below 1423 K for the ss dissolution, and the gradient of the temperature dependence is steeper. There are some possible reasons for the discrepancy between two experiments. They determined the reaction kinetics by measuring the maximum reaction layer growth in the Zry and the ss. As the thickness of the reaction layer was not uniform at high temperatures as shown in Fig.2, it is natural that their study tend to show high reaction rate constants at high temperatures.

One of the major differences in experimental procedures is the heating method. An electric resistance furnace was used in Hofmann's experiments and the heating rate was relatively low, then they started to count the isothermal annealing time when the temperature of a specimen reached 20 K below the predetermined annealing temperature[10]. On the other hand, the holding time at the target temperature was accounted for the isothermal annealing time in the present study in which a rather higher heating rate was achieved by the infrared furnace. Then, the same isothermal annealing condition experimented by us and Hofmann et al. does not mean the same temperature and holding time. The difference can be larger at higher temperatures where the reaction rates are very high, which leads to the difference of the gradient of the temperature dependence.

There was a difference in the evaluation methods. The reaction layer thickness was measured on the horizontal cross section of the reaction couple for reaction kinetics evaluation. As seen in Fig.2, the reaction layer was thicker at the bottom side, and generally the thickness of the reaction layer changed with elevation. It shows that evaluation at different positions or different cutting surfaces produces different results.

Consequently, these differences in the experimental and evaluation procedure between two experiments could cause the discrepancy in the temperature dependence of the reaction rate constants.

4. Conclusions

Reaction couples consisting of Zircaloy-4 and stainless steel type 304 were isothermally annealed in the temperature range from 1273 to 1573 K to obtain the basic information on the melt progress in the fuel bundle during an LWR severe accident.

Reaction layers formed at the interface grew as the temperature and the time increases. Both the materials were dissolved by the reaction, however, the Zircaloy was preferentially dissolved. The SEM/EDX analyses showed that the main process of the of the reaction was diffusion of Fe, Cr, and Ni into the Zry which resulted in the formation of a Zr-rich eutectic through the tested temperature range.

The reaction rate was evaluated for decreases in the thickness of the Zircaloy-4 and the stainless steel, respectively. The reaction generally obeyed a parabolic rate law and the reaction rate constant was determined for every examined temperature. Consequently, an Arrhenius type rate equation was derived respectively for decreases in the Zry and the ss thickness in the examined temperature range. The rate equations are as follows:

for decrease in the Zry thickness;

$$x^2/t\ [m^2/s]=3.11\times10^9 \exp(-496000/RT),\ 1273 \text{ to } 1573 \text{ K}$$

for decrease in the ss thickness;

$$x^2/t\ [m^2/s]=1.79\times10^8 \exp(-445000/RT),\ 1273 \text{ to } 1473 \text{ K}$$

where x is decrease in Zircaloy thickness, t is time, R=8.314 J/mol K, T is given in K, and the activation energies in J/mol.

The obtained rate equations are somewhat different from those reported in the previous study. The discrepancy could be caused by the difference in the experimental and evaluation procedure and the experimental condition.

Reference

(1) Petti, D.A., Martinson, Z.R., Hobbins, R.R., Allison, C.M., Carlson, E.R., Hagrman, D.L., Cheng, T.C., Hartwell, J.K., Vinjamuri, K., and Seifken, L.J.; U.S. Nuclear Regulatory Commission Report, NUREG/CR-5163(1988).

(2) Schanz, G., Hagen, S., Hofmann, P., Schumacher, G., and Sepold, L.; J.Nucl.Mater. 188(1992)131.

(3) Gauntt, R.O., Gasser, R.D. and Otto, L.T.; Sandia National Laboratories Report, SAND86- 1443, NUREG/CR 4671(1989).

(4) Hofmann, P.; U.S.Nuclear Regulatory Commission Report, NUREG/CR-5119(1988).

(5) Jensen, S.M., Akers, D.W., and Pregger, B.A.; OECD LOFT-T-3810(1989).

(6) Uestsuka, H., Nagase, F., and Otomo, T.; Trans. ANS 69(91993)309

(7) Hering, W. and Hofmann, P.; Kernforshungszentrum Karlsruhe report, KfK-5125 (1994)

(8) Bhanumurthy, K., Kale, G.B., and Khera, S.K. J.Nucl.Mater. 185(1991)208

(9) Shaaban, H.I., Hammad, F.H., and Baron,J.L.; J.Nucl.Mater. 71(1978)277

(10) Hofmann, P. and Markiewicz, M.; Kernforschunfszentrum Karlsruhe Report KfK-5106(1994)

(11) Hofmann, P. and Markiewicz, M.; J.Nucl.Mater. 209(1994)92

(12) Kim, K.T. and Olander, D.R.; J.Nucl.Mater. 154(88)102

(13) Massalski, T.B.; Binary alloy phase diagrams, Vol.1, 2, American Society for Metals, Ohio(1986)

(14) Kleykamp, H. and Pejsa, R.; Kernforshungszentrum Karlsruhe Report KfK-4872(1991)

(15) Kubaschewski, O.; Iron-binary phase diagrams, Springer-Verlag, 1982

Table 1 Chemical composition of Zircaloy-4 and stainless steel type 304 in wt%

	Zr	Sn	Fe+Cr	C	Hf	O	H	N
Zircaloy-4	Bal.	1.52	0.3	0.005	<0.005	0.101	<0.002	<0.002

	Fe	Cr	Ni	C	Si	Mn	P	S
stainless steel type 304	Bal.	18.79	8.24	0.06	0.33	1.70	0.032	0.021

Table 2 Results of SEM/EDX analysis of reaction layers formed in reaction couples annealed at 1473 K for 300 s

Reaction layer	Position	Composition (wt%) Zr	Sn	Fe	Cr	Ni	Mn	Si
Zry	**average**	**98.0**	**1.1**	**0.6**	**0.4**			
Layer I	near boundary	75.5	0.8	18.0	1.1	4.0	0.5	
	average	**75.0**	**0.9**	**18.0**	**1.1**	**4.0**	**0.5**	
	10 μ m from boundary	76.3	0.9	12.1	9.2	0.8	0.8	
	Region C (adjacent to boundary)	*35.1*	*0.3*	*29.9*	*32.4*	*0.6*	*1.7*	
Layer II	**average**	**1.1**	**0.2**	**59.9**	**33.7**	**3.3**	**2.0**	
ss	**average**			**68.4**	**19.8**	**8.7**	**2.0**	**1.1**

Table 3 Results of SEM/EDX analysis of reaction layers formed in reaction couples annealed at 1523 K for 60 s

Reaction layer	Position	Composition (wt%) Zr	Sn	Fe	Cr	Ni	Mn	Si
Zry	**average**	**98.0**	**1.1**	**0.6**	**0.4**			
Layer I	near boundary	75.4	0.8	17.0	2.7	3.8		
	average	**74.5**	**1.1**	**17.1**	**3.9**	**2.7**		
	20 μ m from boundary	77.5	1.1	15.7	3.2	2.5		
	Region D (adjacent to boundary)	*37.5*	*0.0*	*37.8*	*21.9*	*1.2*	*1.6*	
Layer II	**average**	**1.9**	**0.1**	**66.8**	**23.0**	**5.1**	**2.2**	**1.0**
	matrix	0.8		65.8	26.7	3.8	2.0	0.9
	grain boundary	26.9		45.3	10.3	15.4		
ss	**average**			**68.4**	**19.8**	**8.7**	**2.0**	**1.1**

Table 4 Results of SEM/EDX analysis of reaction layers formed in reaction couples annealed at 1573 K for 30 s

Reaction layer	Position	Composition (wt%) Zr	Sn	Fe	Cr	Ni	Mn	Si
Zry	**average**	**98.0**	**1.1**	**0.6**	**0.4**			
	Region 1	75.0	1.0	18.0	1.6	3.8	0.6	
	Region 2	76.1	1.0	18.0	2.6	2.9	0.6	
	Region 3	77.6	0.9	16.0	2.5	2.7	0.5	
Layer I	Region 4	54.5	0.7	29.6	11.3	2.9	1.1	
	Region 5	44.7	0.5	36.6	14.0	2.4	1.7	
	Region 6	6.5	0.2	64.7	21.0	5.6	2.0	
	Region 7	14.3	0.3	58.5	17.2	7.2	2.5	
Layer II	**average**	**1.5**	**0.6**	**67.0**	**23.6**	**4.9**	**2.4**	
ss	**average**			**68.4**	**19.8**	**8.7**	**2.0**	**1.1**

Table 5 Reaction rate constants

Temperature	Present study			Hofmann et al. [10]		
	Reaction rate constant (m^2/s)		Time range (s)	Reaction rate constant (m^2/s)		Time range (s)
	Decrease in Zry thickness	Decrease in ss thickness		Decrease in Zry thickness	Decrease in ss thickness	
1273K	6.98×10^{-12}	8.79×10^{-13}	[900 - 28800]	9.48×10^{-12}	5.74×10^{-14}	[300 - 1800]
1323K	9.17×10^{-11}	4.32×10^{-12}	[900 - 14400]			
1373K	6.37×10^{-10}	3.44×10^{-11}	[300 - 3600]	1.44×10^{-9}	8.72×10^{-12}	[120 - 1800]
1423K	3.40×10^{-8}	8.10×10^{-11}	[120 - 1800]	7.69×10^{-9}	3.81×10^{-11}	[60 - 300]
1473K	6.64×10^{-9}	2.46×10^{-10}	[120 - 900]	3.33×10^{-8}	4.79×10^{-10}	[60 - 180]
1523K	3.05×10^{-8}		[30 - 300]			
1573K	6.38×10^{-8}		[30 - 60]			

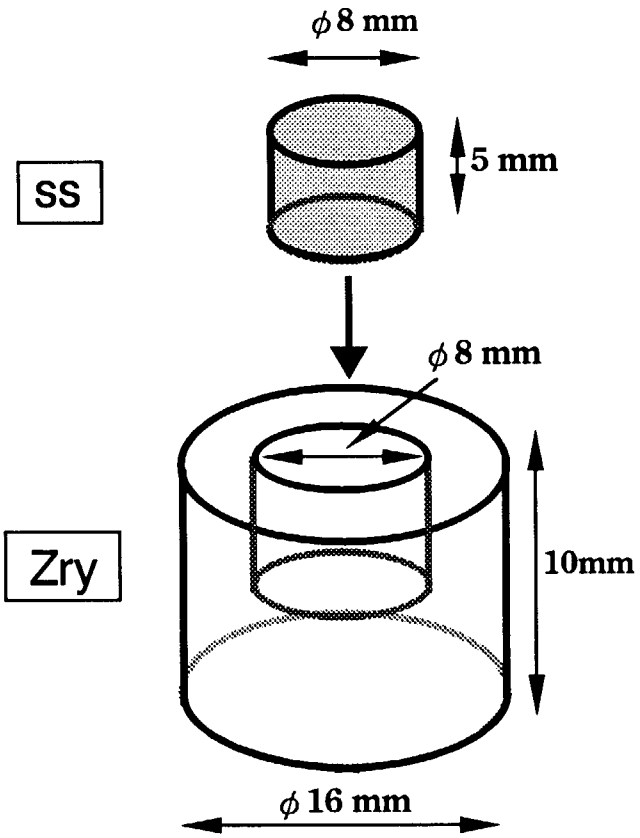

Fig.1 Schematic illustration and geomrtry of the reaction couple

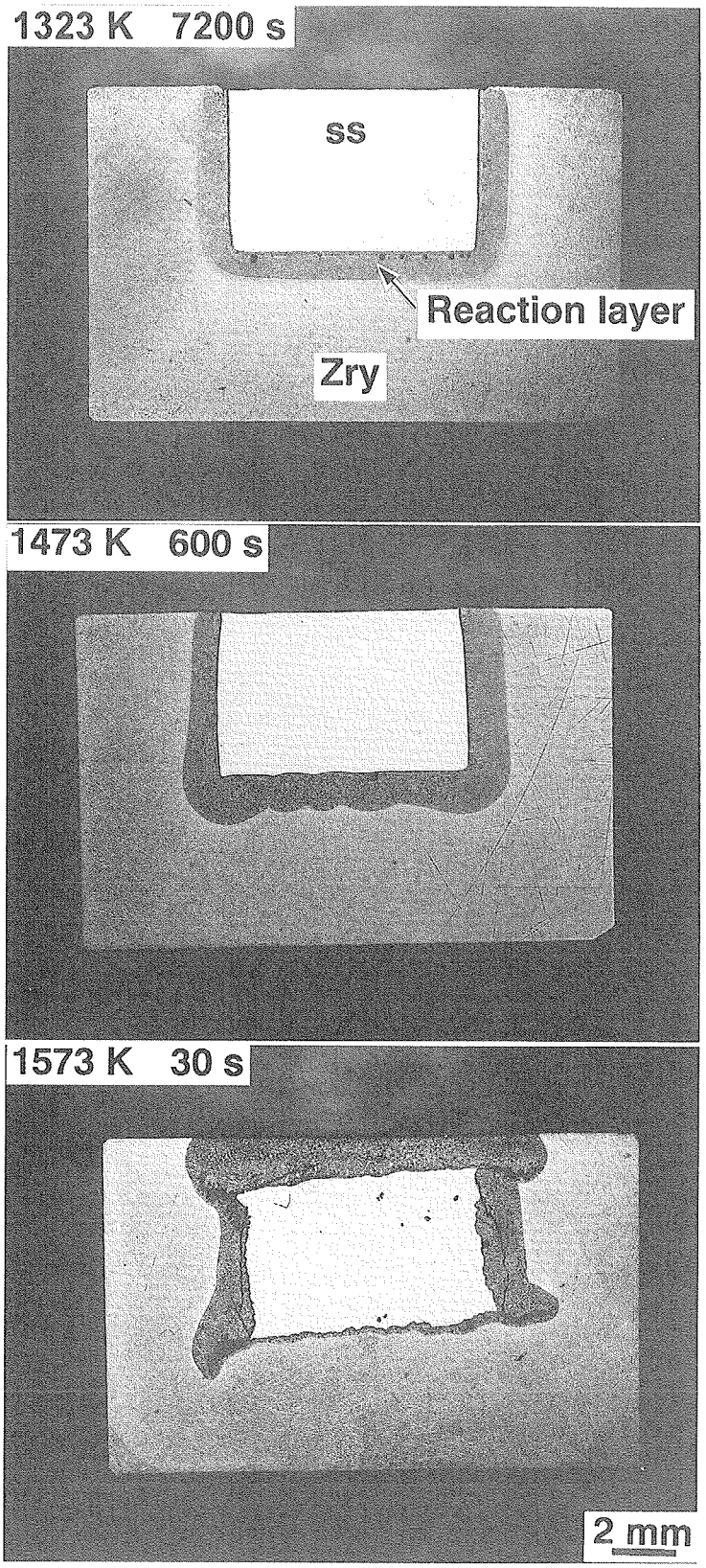

Fig.2 Cross sections of the reaction couples annealed at 1323 K 7200 s, 1473 K for 600 s, and at 1573 K for 30 s

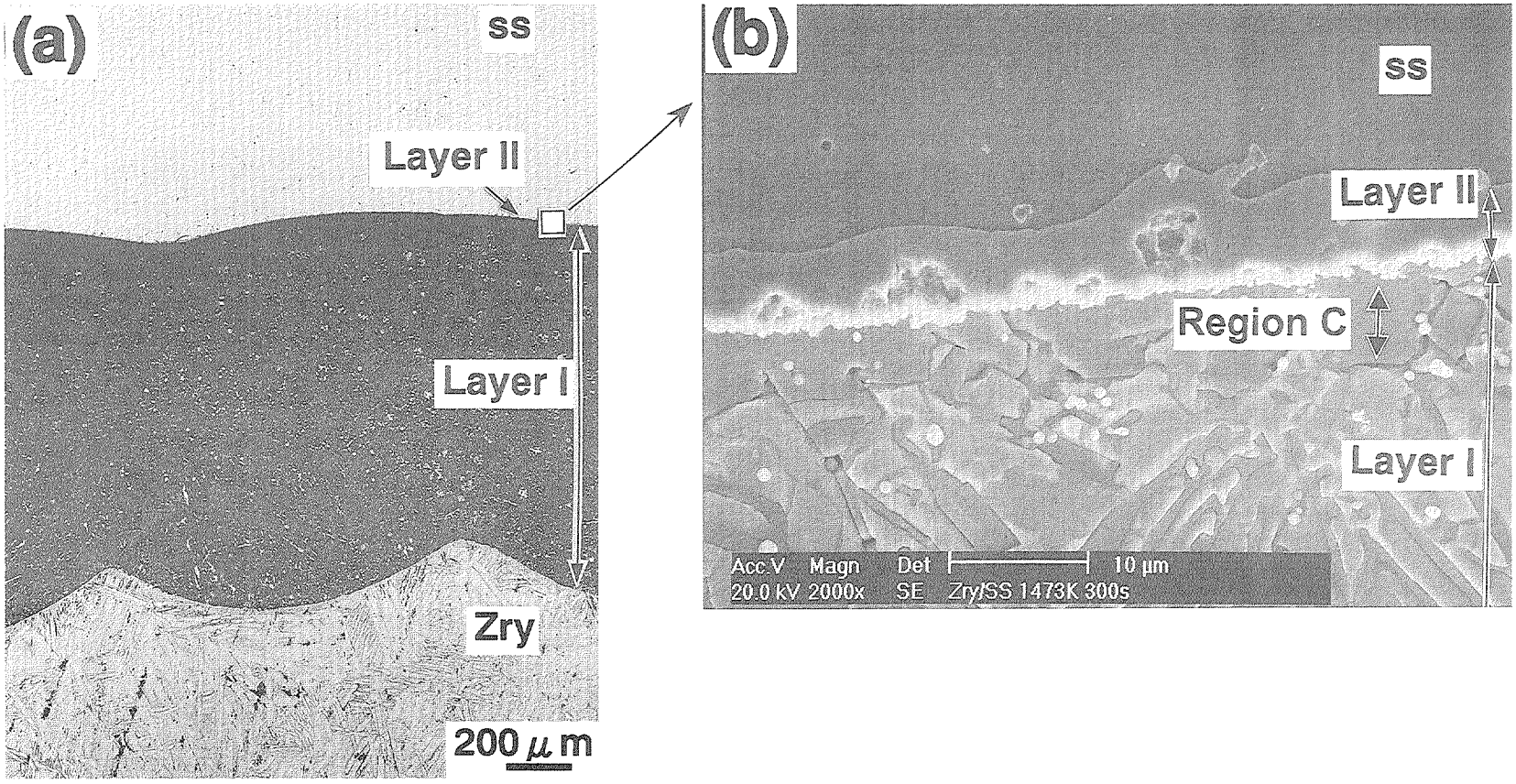

Fig.3 Microstructure of the reaction layers formed in the reaction couple annealed at 1473 K for 300 s

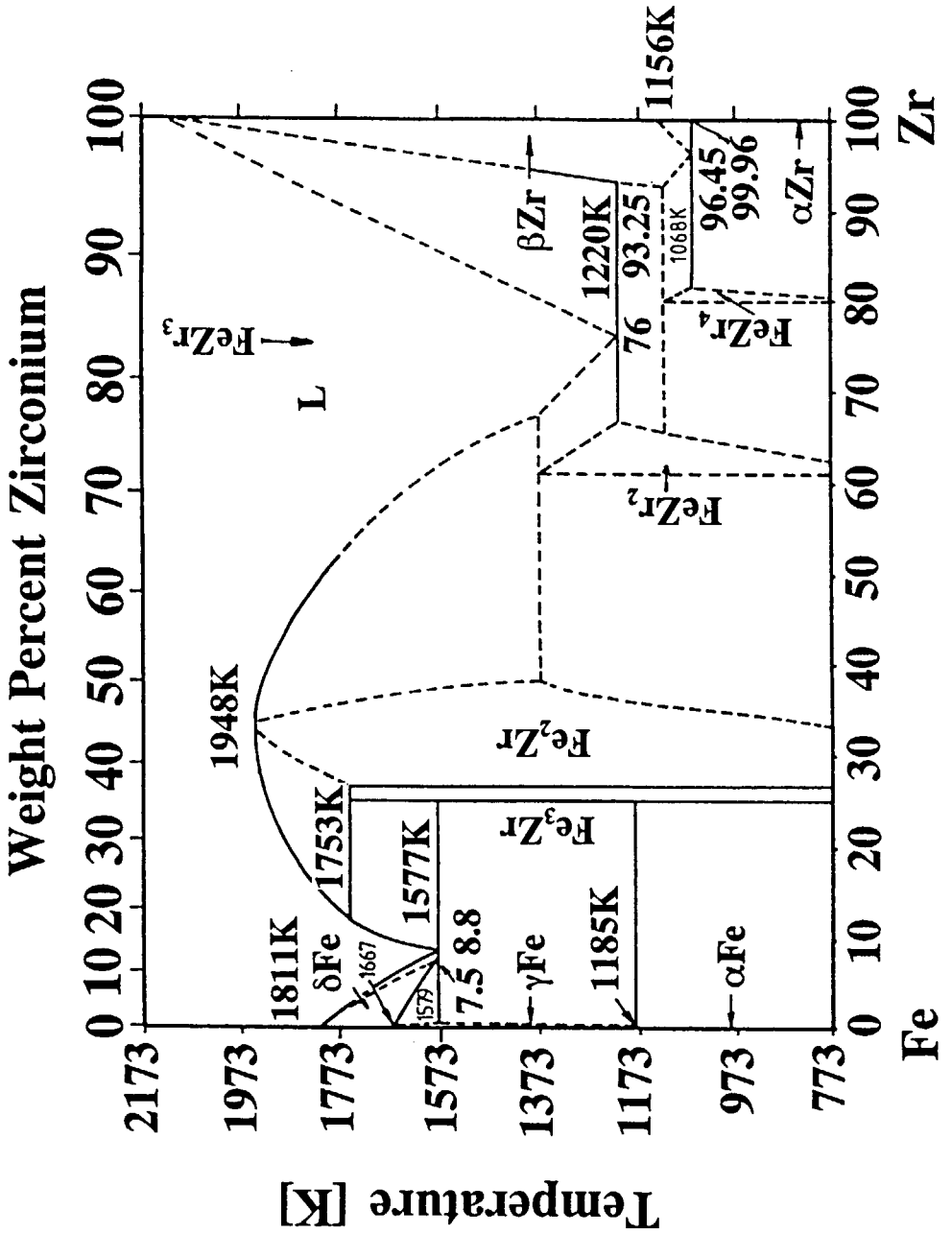

Fig.4 Binary phase diagram of Fe-Zr system [13]

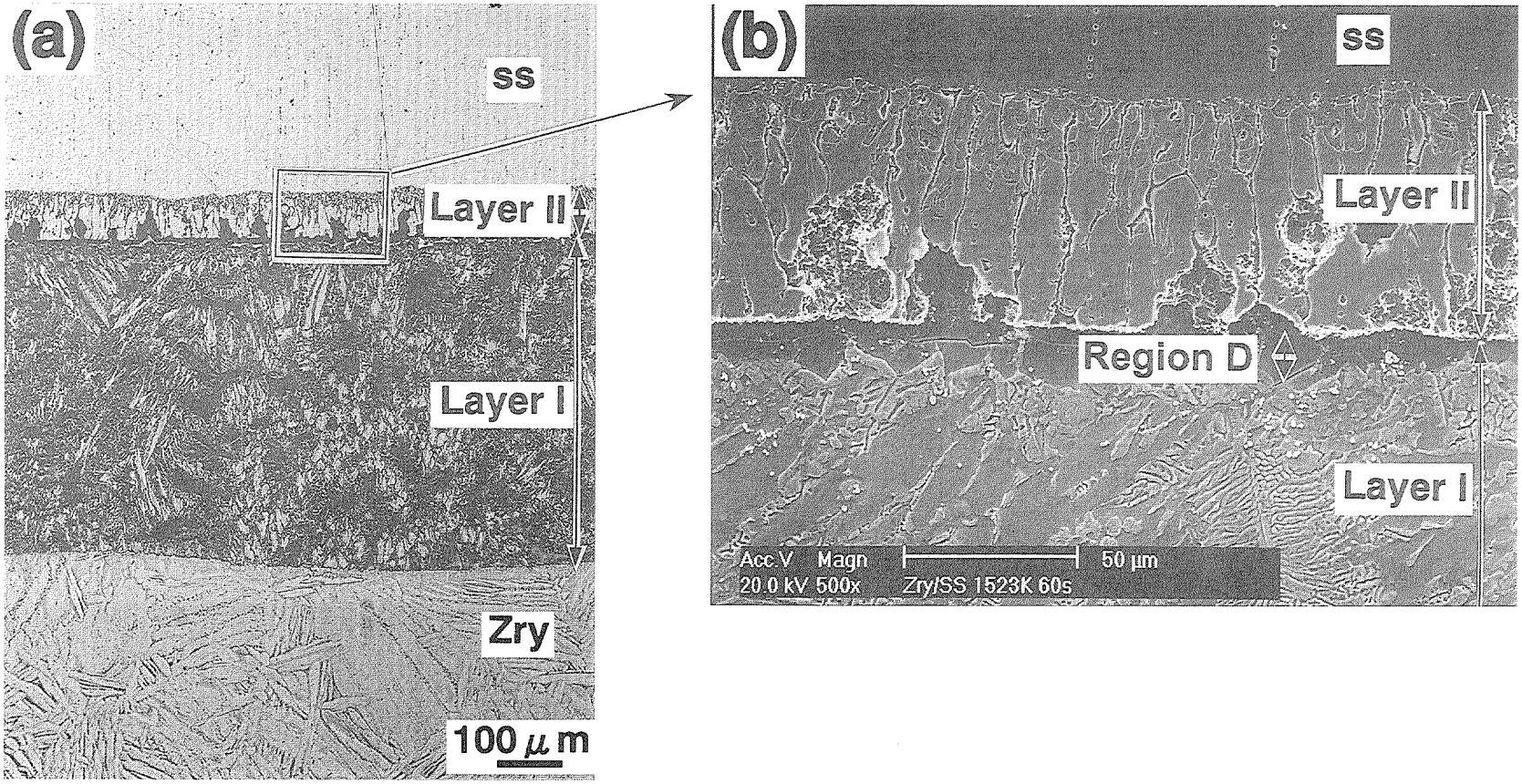

Fig.5 Microstructure of the reaction layers formed in the reaction couple annealed at 1523 K for 60 s

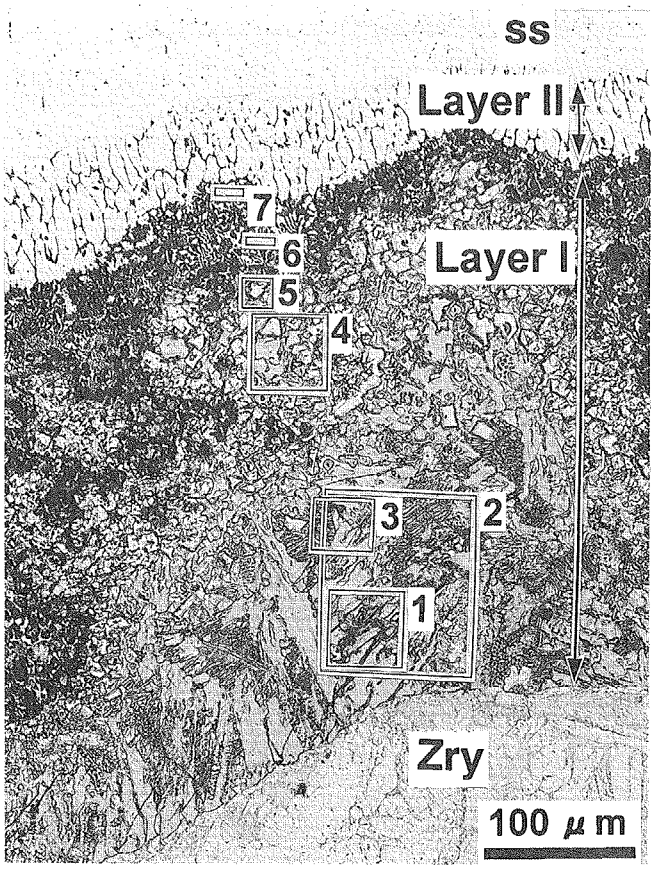

Fig.6 Microstructure of the reaction layers formed in the reaction couple annealed at 1573 K for 30 s

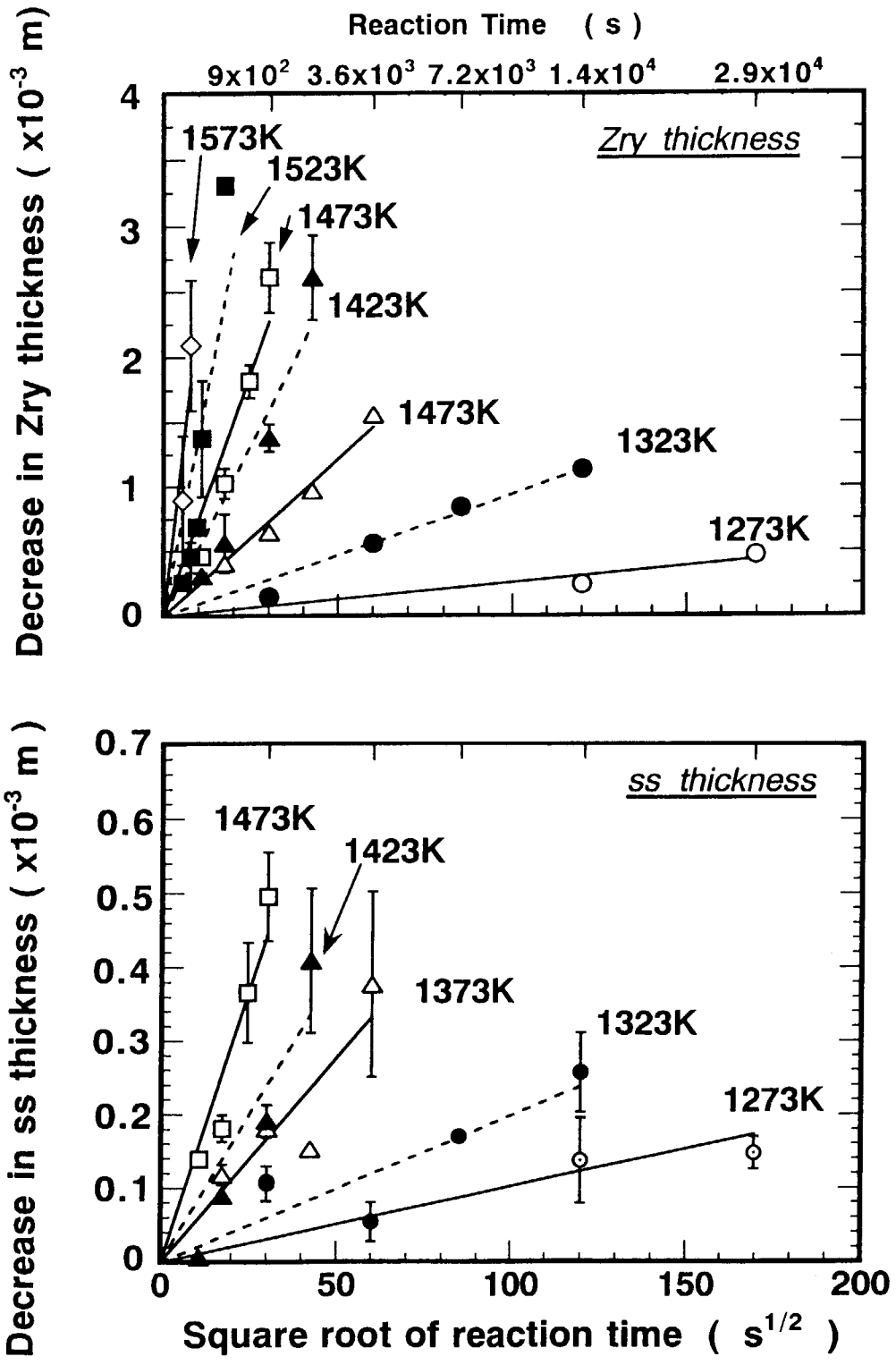

Fig.7 Correlation between decreases in the Zry and the ss thickness and square root of the reaction time

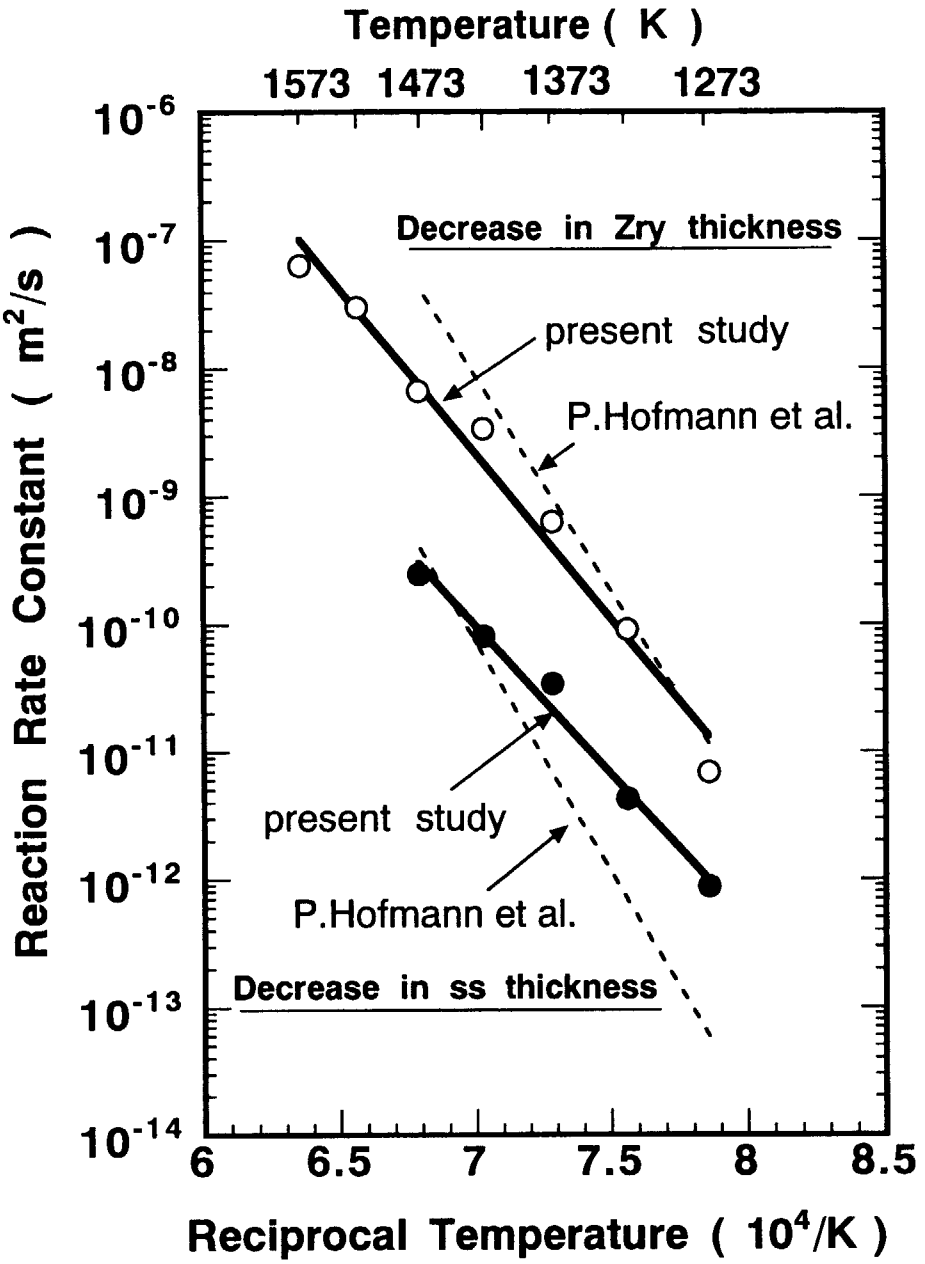

Fig.8 Arrhenius plot of the reaction rate for decreases in the Zry and the ss thickness

This is a blank page.

国際単位系 (SI) と換算表

表 1　SI 基本単位および補助単位

量	名称	記号
長さ	メートル	m
質量	キログラム	kg
時間	秒	s
電流	アンペア	A
熱力学温度	ケルビン	K
物質量	モル	mol
光度	カンデラ	cd
平面角	ラジアン	rad
立体角	ステラジアン	sr

表 2　SI と併用される単位

名称	記号
分，時，日	min，h，d
度，分，秒	°，′，″
リットル	l，L
トン	t
電子ボルト	eV
原子質量単位	u

1 eV = 1.60218 × 10^{-19} J

1 u = 1.66054 × 10^{-27} kg

表 3　固有の名称をもつ SI 組立単位

量	名称	記号	他の SI 単位による表現
周波数	ヘルツ	Hz	s^{-1}
力	ニュートン	N	$m \cdot kg/s^2$
圧力，応力	パスカル	Pa	N/m^2
エネルギー，仕事，熱量	ジュール	J	N·m
工率，放射束	ワット	W	J/s
電気量，電荷	クーロン	C	A·s
電位，電圧，起電力	ボルト	V	W/A
静電容量	ファラド	F	C/V
電気抵抗	オーム	Ω	V/A
コンダクタンス	ジーメンス	S	A/V
磁束	ウェーバ	Wb	V·s
磁束密度	テスラ	T	Wb/m^2
インダクタンス	ヘンリー	H	Wb/A
セルシウス温度	セルシウス度	℃	
光束	ルーメン	lm	cd·sr
照度	ルクス	lx	lm/m^2
放射能	ベクレル	Bq	s^{-1}
吸収線量	グレイ	Gy	J/kg
線量当量	シーベルト	Sv	J/kg

表 4　SI と共に暫定的に維持される単位

名称	記号
オングストローム	Å
バーン	b
バール	bar
ガル	Gal
キュリー	Ci
レントゲン	R
ラド	rad
レム	rem

1 Å = 0.1 nm = 10^{-10} m

1 b = 100 fm^2 = 10^{-28} m^2

1 bar = 0.1 MPa = 10^5 Pa

1 Gal = 1 cm/s^2 = 10^{-2} m/s^2

1 Ci = 3.7 × 10^{10} Bq

1 R = 2.58 × 10^{-4} C/kg

1 rad = 1 cGy = 10^{-2} Gy

1 rem = 1 cSv = 10^{-2} Sv

表 5　SI 接頭語

倍数	接頭語	記号
10^{18}	エクサ	E
10^{15}	ペタ	P
10^{12}	テラ	T
10^{9}	ギガ	G
10^{6}	メガ	M
10^{3}	キロ	k
10^{2}	ヘクト	h
10^{1}	デカ	da
10^{-1}	デシ	d
10^{-2}	センチ	c
10^{-3}	ミリ	m
10^{-6}	マイクロ	μ
10^{-9}	ナノ	n
10^{-12}	ピコ	p
10^{-15}	フェムト	f
10^{-18}	アト	a

（注）

1. 表 1 − 5 は「国際単位系」第 5 版，国際度量衡局 1985 年刊行による。ただし，1 eV および 1 u の値は CODATA の 1986 年推奨値によった。
2. 表 4 には海里，ノット，アール，ヘクタールも含まれているが日常の単位なのでここでは省略した。
3. bar は，JIS では流体の圧力を表わす場合に限り表 2 のカテゴリーに分類されている。
4. EC 閣僚理事会指令では bar，barn および「血圧の単位」mmHg を表 2 のカテゴリーに入れている。

換　算　表

力	N(=10^5 dyn)	kgf	lbf
	1	0.101972	0.224809
	9.80665	1	2.20462
	4.44822	0.453592	1

粘　度　1 Pa·s(N·s/m^2) = 10 P(ポアズ)(g/(cm·s))

動粘度　1 m^2/s = 10^4 St(ストークス)(cm^2/s)

圧力	MPa(=10 bar)	kgf/cm^2	atm	mmHg(Torr)	lbf/in^2(psi)
	1	10.1972	9.86923	7.50062×10^3	145.038
	0.0980665	1	0.967841	735.559	14.2233
	0.101325	1.03323	1	760	14.6959
	1.33322×10^{-4}	1.35951×10^{-3}	1.31579×10^{-3}	1	1.93368×10^{-2}
	6.89476×10^{-3}	7.03070×10^{-2}	6.80460×10^{-2}	51.7149	1

エネルギー・仕事・熱量	J(=10^7 erg)	kgf·m	kW·h	cal(計量法)	Btu	ft·lbf	eV
	1	0.101972	2.77778×10^{-7}	0.238889	9.47813×10^{-4}	0.737562	6.24150×10^{18}
	9.80665	1	2.72407×10^{-6}	2.34270	9.29487×10^{-3}	7.23301	6.12082×10^{19}
	3.6×10^6	3.67098×10^5	1	8.59999×10^5	3412.13	2.65522×10^6	2.24694×10^{25}
	4.18605	0.426858	1.16279×10^{-6}	1	3.96759×10^{-3}	3.08747	2.61272×10^{19}
	1055.06	107.586	2.93072×10^{-4}	252.042	1	778.172	6.58515×10^{21}
	1.35582	0.138255	3.76616×10^{-7}	0.323890	1.28506×10^{-3}	1	8.46233×10^{18}
	1.60218×10^{-19}	1.63377×10^{-20}	4.45050×10^{-26}	3.82743×10^{-20}	1.51857×10^{-22}	1.18171×10^{-19}	1

1 cal = 4.18605 J（計量法）

= 4.184 J　（熱化学）

= 4.1855 J　（15 °C）

= 4.1868 J（国際蒸気表）

仕事率　1 PS（仏馬力）

= 75 kgf·m/s

= 735.499 W

放射能	Bq	Ci
	1	2.70270×10^{-11}
	3.7×10^{10}	1

吸収線量	Gy	rad
	1	100
	0.01	1

照射線量	C/kg	R
	1	3876
	2.58×10^{-4}	1

線量当量	Sv	rem
	1	100
	0.01	1

（86 年 12 月 26 日現在）